T cell polarization and NFAT translocation are stiffness-dependent and are differentially regulated by Piezo1 and Orai1

Renping Zhao[1], Jingnan Zhang[2], Eva C. Schwarz[1], Aránzazu del Campo[2,3], Markus Hoth[1], Bin Qu[1*]

[1] Biophysics, Center for Integrative Physiology and Molecular Medicine (CIPMM), School of Medicine, Saarland University, Homburg, Germany
[2] INM - Leibniz Institute for New Materials, Saarbrücken, Germany
[3] Chemistry Department, Saarland University, Saarbrücken, Germany

* Bin Qu.

Email: bin.qu@uks.eu

Author Contributions: RZ performed the experiments and the corresponding analysis if not mentioned otherwise; JZ prepared hydrogels; MH, ECS, and AdC helped with data interpretation and provided critical feedback on all aspects of the project; Together with RZ and MH, BQ generated concepts and wrote the manuscript; All authors contributed to the writing, editing and cross-checking of the manuscript.

Competing Interest Statement: The authors declare that the research was conducted in the absence of any commercial or financial relationships that could be construed as a potential conflict of interest.

Classification: Biological Sciences/Cell Biology

Keywords: T cells, Mechanosensing, Piezo1, stiffness, T cell polarization, Ca^{2+} influx

Abstract

Effective T cell responses against tumor cells require diverse effector functions including polarization towards tumor cells to form immunological synapses and nuclear factor of activated T-cells (NFAT)-dependent gene transcription. While the role of tumor cell softening has been associated with malignancy, stemness, and metastasis, potentially contributing to immune evasion, its impact on cellular processes in T cells is not well understood. Here, we show that both T cell polarization and NFAT nuclear translocation are modulated by target stiffness in a Ca^{2+} dependent manner. Using both anti-CD3 antibody-functionalized substrates with varying stiffness as surrogates for target cells or softened tumor cells, we found that both, reorientation of microtubule organizing center (MTOC) towards the tumor cells, a hallmark for T cell polarization, and NFAT translocation were impaired on softer hydrogels or following contact with softer cancer cells. The amplitudes of intracellular Ca^{2+} signals were dependent on stiffness, and removal of extracellular Ca^{2+} inhibited stiffness-dependent T cell responsiveness. While stiffness-dependent Ca^{2+} signaling was crucial for both, T cell polarization and NFAT translocation, Ca^{2+} influx through Piezo1, a mechanosensitive ion channel, mediated stiffness-dependent MTOC reorientation but not NFAT translocation. In contrast, Ca^{2+} influx through store-operated Orai channels mediated NFAT translocation but not MTOC reorientation. Our results demonstrate that tumor cell stiffness directly influences T cell functionality through distinct Ca^{2+} influx pathways, revealing cell softening as an essential mechanism employed by malignant cells to evade immune surveillance.

Introduction

One significant challenge that immune cells face within the solid tumor microenvironment is the phenomenon of cancer cell softening, a characteristic linked to increased malignancy, metastasis, and stemness. Compelling evidence at the single-cell level, derived from both optical stretching methods and atomic force microscopy, highlights that carcinoma cells, including those from breast, cervix, and ovarian cancers, exhibit greater deformability with lower Young's moduli in comparison to their non-malignant counterparts [1, 2, 3, 4]. Among cancerous cells, those displaying softer mechanical properties exhibit increased invasiveness, higher potentials to establish metastatic clones, and an up-regulation of gene profiles associated with stemness [2, 5, 6]. Moreover, when malignant cancer cells navigate confined channels, they can undergo further softening [6]. However, the extent to which cancer cell softening facilitates the evasion of immune surveillance by malignant cells remains poorly understood.

As a crucial component of immune responses against cancer, T cells must promptly and robustly respond to stimuli, with activation needing to be precisely tuned, either propagated or terminated, to effectively eliminate cancer cells without compromising healthy cells or tissues. Upon identifying cognate target cells, the cytoskeleton of T cells undergoes polarization towards these targets, ensuring the specific delivery of vesicles containing cytokines or cytotoxic proteins [7, 8]. A fundamental rearrangement of the cytoskeleton involves the rapid translocation of the microtubule-organizing center (MTOC) towards the target cells, acting as a hallmark for the formation of the immunological synapse (IS) and playing a pivotal role in subsequent effector functions [9, 10, 11]. In T cells, the failure of MTOC reorientation towards the IS is associated with the lack of enrichment of lytic granules, significantly impaired lytic capability [12, 13], and reduced IL-2 production [14]. For further T cell commitment, gene regulation by nuclear factor of activated T cells (NFAT) plays a central role in T cell fate determination, either sustaining T cells in an activated state or reprogramming T cells into an unresponsive state [15, 16]. NFAT activity depends on its translocation from the cytosol into the nucleus following TCR activation [15, 16, 17].

The elevation of intracellular calcium (Ca^{2+}) levels ($[Ca^{2+}]_{int}$) is a hallmark of T cell activation, and the resulting $[Ca^{2+}]_{int}$ increase triggered by target recognition plays a pivotal role in both NFAT nuclear translocation and MTOC polarization. In the resting state, NFAT resides in the cytosol in its phosphorylated form; upon activation, Ca^{2+}-dependent calcineurin dephosphorylates NFAT proteins, enabling their translocation to the nucleus [18, 19, 20]. Deficiencies in store-operated Ca^{2+} entry (SOCE) in T cells impede NFAT activation, hindering nuclear translocation following IS formation [21, 22]. Although the role of Ca^{2+} in MTOC polarization is not entirely elucidated, the absence of extracellular Ca^{2+} has been observed to diminish MTOC translocation in response to target cells [23, 24]. Interestingly, chelation of both extracellular and intracellular Ca^{2+} significantly impairs MTOC translocation [10] but removal of intracellular Ca^{2+} with BAPTA does not affect MTOC repositioning [13].

Store-operated Ca^{2+} entry (SOCE) is the primary Ca^{2+} influx mechanism in T cells [25, 26]. Upon the recognition of target cells, TCR activation initiates the production of inositol trisphosphate (IP_3), which binds to its receptor IP_3R at the endoplasmic reticulum (ER), prompting the efflux of Ca^{2+} from the ER into the cytosol [27]. Ca^{2+} depletion in the ER is sensed by stromal interaction molecules (STIM) and the clustering of STIM in the ER membrane activates calcium release-activated calcium (CRAC) channels called Orai, allowing the entry of extracellular Ca^{2+} [28, 29]. Defects in Orai proteins in patients are associated with severe immunodeficiency due to the failure of T cell activation [30, 31, 32].

Ca^{2+} entry can also be mediated by other ion channels, including Piezo1. Piezo1 is a trimeric mechanosensitive cation channel and is permeable to Ca^{2+} [33, 34]. In T cells, the activation of Piezo1 induces Ca^{2+} influx, and the downregulation of Piezo1 hampers the activation and proliferation of T cells [35]. *In vivo*, Piezo1 deficiency promotes the expansion of regulatory T cells, thereby

attenuating the severity of experimental autoimmune encephalomyelitis, a mouse model for multiple sclerosis [36]. Piezo1 is also implicated in the regulation of integrin-dependent chemotaxis [37] and the shear stress-enhanced activation of T cells [38].

In this study, we show that decreased substrate stiffness or softer tumor cells impair the responsiveness of T cells, as evident from Ca^{2+} influx, NFAT nuclear translocation, and MTOC reorientation towards the IS. Both Orai1 and Piezo1 contribute to the IS formation-triggered Ca^{2+} entry in a stiffness-dependent manner. Piezo1 plays a crucial role in the rapid increasing phase, while Orai1 is more important for the sustainability of elevated intracellular Ca^{2+} concentrations. Orai1-mediated Ca^{2+} entry is required for NFAT nuclear translocation, as expected from the literature [21, 22] but, unexpectedly, not for MTOC reorientation. On the opposite, Piezo1-mediated fast Ca^{2+} increases primarily influence MTOC reorientation, with no discernible impact on NFAT nuclear translocation. These findings assign specific functions to Ca^{2+} influx by Orai and Piezo1, unveiling a hitherto unreported intrinsic mechanism that coordinates the rapid and long-term cellular responses to stiffness cues.

Results

Several key processes collectively optimize and modulate efficient T cell responses against pathogens or cancer. Among those, MTOC reorientation to the immunological synapse (IS) is a pivotal event during T cell polarization, and NFAT nuclear translocation is essential to initiate gene transcription programs. Given that T cells are exposed to varying levels of stiffness in their microenvironment, we analyzed how different stiffness levels of 2, 16, and 64 kPa, covering the physiological range [39], influence T cell responses. We used the human T cell line Jurkat as a model system and settled them on functional hydrogels of different stiffness (Fig. 1a), which were coated with anti-CD3 antibodies to activate T cell receptors (TCRs), the main initiators of IS formation and T cell signaling. T cells were fixed at different time points, and we analyzed MTOC localization or NFAT translocation. In Fig. 1b and Supplementary Fig. 1, it is evident that MTOC stained with anti-tubulin antibody was consistently closer to the IS at all time points at medium (16 kPa) and stiff (64 kPa) substrates compared to soft ones (2 kPa). Similarly, NFAT translocation to the nucleus stained with Hoechst was fastest at 64 kPa, as observed in the respective fluorescence images and the corresponding quantification (Fig. 1c, d). Given the amounts of anti-CD3 antibodies on the different surfaces were very similar for 2, 16, and 64 kPa (Supplementary Fig. 2), the stiffness of the substrates is the sole differing parameter under these experimental conditions. Our results thus suggest that substrate stiffness modulates both, MTOC reorientation and NFAT nuclear translocation.

We further explored the impact of tumor cell softening on T cell responses. We softened NALM-6 tumor cells by chelating intracellular Ca^{2+} with EGTA-AM. The stiffness of NALM-6 cells was assessed using real-time deformability cytometry (RT-DC), a high throughput technique that quantifies cell deformation along with cell size as cells pass through narrow channels [40]. In comparison to control cells, EGTA-AM-loaded NALM-6 cells exhibited slightly enhanced deformation (Supplementary Fig. 3a) and correspondingly moderately reduced Young's moduli (Supplementary Fig. 3b). We conjugated softened NALM-6 tumor cells with T cells and analyzed MTOC reorientation in T cells. We found that the moderate reduction in the stiffness of EGTA-loaded target cells significantly increased the distance between the MTOC and the IS in the conjugated T cells (Fig. 1e), indicating impaired MTOC translocation towards the IS. Thus, we conclude that target cell stiffness plays a pivotal role in regulating T cell functionality triggered by TCR activation.

Given the crucial role of Ca^{2+} influx in NFAT translocation [19, 20, 21, 22] and its modulation by stiffness as shown above, we hypothesized that stiffness-dependent changes in Ca^{2+} influx may also underlie the modulation of MTOC reorientation. For assessing intracellular Ca^{2+} levels ($[Ca^{2+}]_{int}$),

we utilized functionalized polyacrylamide (PA) hydrogels prepared on coverslips to allow Ca^{2+} imaging. Instead of 2, 16 and 64 kPa, we opted for 2, 12 and 50 kPa, because these conditions have been optimized previously for comparable anti-CD3 antibody coating efficiency for this setting [41]. Supplementary Fig. 4 confirmed the successful formation of a functional IS between T cells and the antibody-functionalized hydrogels, as evident by F-actin localization, CD3 localization, and ZAP-70 phosphorylation (Supplementary Fig. 4). Regarding T cell responsiveness, we noted that stiffer hydrogels correlated with higher proportions of T cells displaying a responsive behavior, characterized by an elevation in $[Ca^{2+}]_{int}$ (Fig. 2a). Among the responsive T cells, $[Ca^{2+}]_{int}$ was substantially higher on stiffer hydrogels compared to those of medium and soft rigidity, as illustrated by three representative examples (Fig. 2b), and the average response of all analyzed cells (Fig. 2c). This stiffness-dependent changes in Ca^{2+} responses are also reflected by rate of $[Ca^{2+}]_{int}$ increase (Fig. 2d), the peak (Fig. 2e), and the plateau (Fig. 2f). For medium and high stiffness levels, $[Ca^{2+}]_{int}$ remained elevated throughout the measurement. While control experiments with CD28 antibody-coated hydrogels induced T cell spreading (Supplementary Fig. 5a) to similar levels as seen with CD3 antibody-functionalized hydrogels, no $[Ca^{2+}]_{int}$ increase was observed on any of the CD28 antibody-functionalized substrates (Supplementary Fig. 5b). This confirms that Ca^{2+} signals were triggered by CD3 engagement and TCR activation, rather than simply by T cell adhesion to the surface. In addition, we found that inhibiting Ca^{2+} influx by chelating extracellular Ca^{2+} significantly compromised TCR activation-induced MTOC reorientation (Fig. 2g). Collectively, our data suggest that $[Ca^{2+}]_{int}$ increases by Ca^{2+} influx plays a critical role in regulating T cell functionality in response to stiffness cues.

To identify the underlying Ca^{2+} channels, we first focused on Orai1 as a potential candidate. Orai1 is the predominantly expressed Ca^{2+} release-activated Ca^{2+} (CRAC) channel in T cells and mediates the major proportion of Ca^{2+} influx. It is well-established that Orai1-dependent Ca^{2+} influx governs NFAT nuclear translocation and activity in T cells [42, 43, 44]. To inhibit Orai1 function, we employed BTP-2 (2-aminoethyl diphenylborinate), a dose-dependent inhibitor primarily targeting CRAC/Orai1 channels [45]. We verified that at a very high concentration (10 µM), BTP2 completely eliminated SOCE through CRAC/Orai1 channels activated by thapsigargin-induced store depletion (Supplementary Fig. 6) as reported previously [45, 46]. Interestingly, while the inhibition of Orai1 channels by BTP2 completely abolished NFAT nuclear translocation for all three substrate stiffness levels (Fig. 3a), it had no impact on MTOC reorientation or its modulation by stiffness (Fig. 3b). Surprisingly, we found that CD3-induced Ca^{2+} signals were not completely inhibited by BTP2 on stiff (50 kPa) substrates as evident in the examples shown in Figs. 3c and d. Quantification revealed that BTP2 application under these conditions resulted in more transient $[Ca^{2+}]_{int}$ signals with similar increase rates (Fig. 3e), peak values (Fig. 3f) but reduced $[Ca^{2+}]_{int}$ over longer times (Fig. 3g). A similar effect of BTP2 was also found for the medium stiffness (12 kPa, Supplementary Fig. 7). Our findings suggest that sustained $[Ca^{2+}]_{int}$ by CRAC/Orai1 plays a critical role for NFAT nuclear translocation, however, another stiffness-regulated Ca^{2+} influx pathway must mediate MTOC reorientation.

Mechanosensitive ion channels are crucial for adapting T cell behaviour to mechanical cues and many of these channels are Ca^{2+} permeable [39, 47]. Among those channels, we identified Piezo1 as the most predominantly, if not the sole mechanosensitive ion channel expressed in Jurkat and primary human $CD4^+$ T cells, as revealed by RNA sequencing analysis (Fig. 4a). To investigate whether Piezo1 regulates Ca^{2+} entry in T cells, we downregulated Piezo1 using siRNA (Supplementary Fig. 8). Its downregulation resulted in reduced Ca^{2+} influx, as shown in the examples (Fig. 4b, c) and quantified by $[Ca^{2+}]_{int}$ increase rates (Fig. 4d), peak levels (Fig. 4e), and plateau levels (Fig. 4f). These findings show that Piezo1 is involved in initiation of Ca^{2+} influx upon TCR activation and is mainly contributing to the fast-rising phase.

Next, we examined the role of Piezo1 in T cell polarization. In clear contrast to the inhibition of Orai1 channels, inhibition of Piezo1, either by siRNA (Fig. 5a) or its inhibitor GsMTx4 (Fig. 5b), abolished the dependence of MTOC reorientation on stiffness. Similarly, in primary human $CD4^+$ T

cells, GsMTx4 treatment substantially impaired MTOC repositioning towards IS (Fig. 5c). Consistently, for T cells conjugated with superantigen SEA/SEB-pulsed target cells, perturbation of Piezo1, either by siRNA or GsMTx4, also impaired MTOC reorientation induced by target cell recognition as evident from the increase between MTOC and IS (Fig. 5d, e). In addition, activation of Piezo1 by its specific agonist Yoda-1 increased $[Ca^{2+}]_{int}$ (Fig. 5f) and reduced the MTOC-IS distance significantly on 2 kPa with a slight trend for the other levels of stiffness (Fig. 5g). Consistently, results from live-cell imaging show that inhibition of Piezo1 by GsMTx-4 delayed the initiation of MTOC translocation towards the IS and increased the minimal distance between MTOC and IS (Fig. 5h, i). In contrast, when CRAC/Orai1 channels were inhibited by BTP-2, MTOC reorientation was similar compared to control (Fig. 5h, i). Notably, NFAT translocation to the nucleus, was unaffected by Piezo1 (Fig. 5j). These findings suggest that Piezo1-mediated mechanosensing plays a critical role in MTOC reorientation and concomitant T cell polarization without interfering with NFAT nuclear translocation. Collectively, we conclude that Piezo1 governs dynamics of MTOC translocation in response to stiffness.

In summary, our findings establish Piezo1 as a mechanosensor in T cell, governing MTOC reorientation and concurrent polarization. However, its Ca^{2+} signals do not contribute to NFAT translocation. In contrast, beyond its known role in guiding NFAT translocation [21, 22], Orai1 serves as a key regulator for stiffness-dependent modulation of NFAT translocation but is not involved in MTOC reorientation.

Discussion

Decreased cell stiffness is a prominent physical characteristic observed in malignant cells, particularly pronounced in tumor stem cells [1, 2, 3, 4, 5, 6]. Our results demonstrate that softer stiffness levels lead to diminished T cell responsiveness, as evident by smaller fractions of responding cells, reduced Ca^{2+} influx, impaired MTOC reorientation, and NFAT nuclear translocation. Our findings indicate that the inherent softening in tumor cells can significantly diminish corresponding T cell responses, substantially increasing their likelihood of evading immune surveillance and facilitating metastasis and the establishment of clones in distant locations.

How do T cells discern variations in target cell stiffness and respond to this mechanical cue? TCRs inherently respond to mechanical forces generated during engagement with antigens [41, 48], facilitating the exposure of more binding sites to high-affinity antigens [49, 50]. In this context, when interacting with softer tumor cells, the forces generated from bound antigen-TCR complexes are likely smaller compared to those in interactions with stiffer tumor cells. This disparity could plausibly lead to decreased activation of TCR downstream signals including SOCE via Orai channels, thus influencing NFAT activation and its regulated genes to govern T cell fate. We show that inhibiting SOCE with BTP-2 treatment has no impact on the peak levels of $[Ca^{2+}]_{int}$ induced by CD3 antibody coating on substrates. However, when stimulated by soluble CD3 antibody, BTP-2-treated Jurkat T cells exhibit reduced $[Ca^{2+}]_{int}$ peak levels [45]. These findings suggest that SOCE plays a substantial role in the initial Ca^{2+} influx triggered by global stimulation with soluble CD3 antibody, however, SOCE may not be a primary contributor to the initial Ca^{2+} influx induced by stimulation on substrates with physiological levels of stiffness.

To mount an effective immune response against tumor cells, T cells must swiftly engage with recognized target cells and form a functional IS to exert their effector function. MTOC reorientation towards the IS is crucial for T cells to exert their effector functions, as MTOC reorientation plays a pivotal role in both sustaining T cell signaling [14] and facilitating effective directional delivery of vesicles containing cytotoxic proteins or cytokines [51, 52]. Regarding MTOC repositioning upon IS formation, our results show that Piezo1-regulated Ca^{2+} influx plays a key role, establishing a link between Piezo1-mediated mechanosensing and MTOC repositioning. It is reported that MTOC reorientation relies on dynein activity, particularly the formation of dynein ring-like structures at the

IS [10, 53]. MTOC translocation is significantly impaired when dyneins fail to form ring-like structures following IS formation [53]. Although CRAC channel-regulated Ca^{2+} influx in T cells is proven to be essential for various key processes during IS formation including actin reorganization [54], our results show that blocking CRAC channels does not alter activation-triggered MTOC repositioning, suggesting that MTOC reorientation is independent of SOCE-regulated actin reorganization.

Besides rapid responses like MTOC reorientation, subsequent long-term responses are also essential for T cell function, including cytokine production, checkpoint molecule expression, and cell fate determination involving activation, proliferation, and differentiation [55, 56], which together define the potential of subsequent reactions and the destiny of T cells. These responses are regulated by activation and nuclear translocation of the corresponding transcription factors. NFAT proteins play a central role in T cell commitment. Our results show that for Jurkat T cells, CD3 antibody stimulation-induced translocation of NFAT1 into the nucleus is stiffness dependent and regulated by CRAC/Orai-mediated Ca^{2+} influx, but independent of Piezo1. A recent study has reported that fluid shear stress potentiates activation of Jurkat T cells induced by CD3/CD28 antibody-coated beads as evidenced by several early- and late-stage activation markers including NFAT nuclear translocation [38]. One landmark of this shear stress-enhanced T cell activation, ZAP70 phosphorylation, is primarily regulated by Piezo1 and can be abolished by removal of extracellular Ca^{2+} [38]. Considering our findings, shear stress-potentiated NFAT translocation should be independent of Piezo1 but regulated by CRAC/Orai1 channels. Interestingly, in microglial cells, considered the major immune cell type in the brain, activation of NFAT proteins is also independent of Piezo1 [57]. In many other cell types, however, we noticed that Piezo1-mediated mechanosensing is linked to activation of the NFAT family, including macrophages [58], osteoblasts [59], erythroblasts [60], colon cancer stem-like cells [61], and cardiomyocytes [62]. This suggests that different cell types adapt their mechanosensing pathways, with or without Piezo1 involvement, to govern mechanical cue-regulated NFAT nuclear translocation and its related gene regulation.

Rapid responses directly dictate the short-term functionality of T cells during contacts. Subsequently, T cells need to decide whether to sustain or halt their effector function depending on the surrounding microenvironment. For example, if the initially recognized target cell is surrounded by healthy cells, T cells should promptly cease their effector functions to avoid jeopardizing innocent bystander cells. On the other hand, if numerous other target cells are present, T cells should continue their effector functions for efficient elimination. Dysregulation in long-term responses can lead to inappropriate overactivation or suppression of T cell functions, resulting in autoimmune diseases or cancer. Consequently, decoupling rapid and long-term responses is crucial. Our results suggest that T cells employ stiffness as a regulatory cue to coordinate rapid and long-term responses via Piezo1 and Orai1.

In summary, our findings highlight the central role of target cell stiffness in regulating T cell functionality, including both rapid responses and long-term functions. The Ca^{2+} influx triggered by TCR activation emerges as a crucial factor for stiffness sensing. Differential regulation of stiffness-regulated rapid and long-term responses to stiffness is provided by Piezo1 and Orai1, which selectively control distinct mechano- and Ca^{2+}-dependent processes. In addition, our results suggest that mechanosensing may act as a gatekeeper mechanism, setting a threshold below which T cell functions are completely inhibited. As soon as this threshold is exceeded, the T cells are sensitized so that they can react quickly and robustly. This delicate balance could ensure that T cells remain quiescent in non-diseased situations, preventing overreactions to harmless stimuli. Finally, our results provide direct evidence of how tumor cells exploit this stiffness-regulated mechanism to evade immune surveillance. Our data thus support the hypothesis that targeting the mechanosensitivity of T cells could potentially improve the efficacy of immunotherapy [63, 64].

Materials and Methods

Antibodies and reagents

All chemicals not specifically mentioned are from Sigma-Aldrich (highest grade). The following antibodies or reagents were used: Anti-γ-Tubulin antibody (Merck, T5192), Anti-Phospho-Zap-70 (Tyr319)/Syk (Tyr352) (Cell Signaling Technology, 27175), Anti-PIEZO1 (Thermo Fisher Scientific, PA5-72974), Alexa Fluor Plus 488 Goat anti-Rabbit IgG (H+L) Secondary Antibody (Thermo Fisher Scientific, A32731), Alexa Fluor™ 647 Goat anti-Rabbit IgG (H+L) Secondary Antibody (Thermo Fisher Scientific), Alexa Fluor™ 568 Goat anti-Rabbit IgG (H+L) Secondary Antibody (Thermo Fisher Scientific, A-11036), Alexa Fluor® 647 anti-human human CD3 Antibody (BioLegend, 300416), Biotin anti-human CD3 Antibody (BioLegend, 317320), Biotin anti-human CD28 Antibody (BioLegend, 302904), Alexa Fluor® 647 anti-Tubulin-α Antibody (BioLegend, 627908), Fura-2/AM (Thermo Fisher Scientific, F1221), Fluo-4/AM (Thermo Fisher Scientific, F14201), SPY650-tubulin (Spiochrome, SC503), Hoechst 33342 (ThermoFisher Scientific, H3570), fibronectin (Sigma-Aldrich, F4759), Poly-L-ornithine (Sigma-Aldrich, P3655).

Cell culture and transfection

Jurkat T cells (Clone E6-1, from ATCC), Raji (from DSMZ) and NALM-6 cells (kindly provided by Adolfo Cavalié, Saarland University) were cultured in RPMI 1640 (ThermoFisher Scientific) supplemented with 10% fetal calf serum (ThermoFisher Scientific) and 1% penicillin–streptomycin (ThermoFisher Scientific). Primary human $CD4^+$ T cells were isolated from peripheral blood mononuclear cells obtained from healthy donors using Human $CD4^+$ T Cell Isolation Kit (Miltenyi Biotec) according to the manual, and were stimulated with Dynabeads™ Human T-Activator CD3/CD28 (ThermoFisher Scientific) with 30 U/ml of recombinant human IL-2 (Miltenyi Biotec). T cells were cultured in AIMV (ThermoFisher Scientific) with 10% fetal calf serum and 1% penicillin–streptomycin. All cells were cultured at 37°C, 5% CO_2 in a humidified incubator. Jurkat T cells were transfected with ON-TARGETplus SMARTpool human Piezo1 siRNA or control siRNA (Horizon Discovery, previously Dharmacon) with SE Cell Line 4D-Nucleofector™ X Kit (Lonza). Jurkat T cells were used for the experiment after 24 h.

Fluorescence-based Ca^{2+} imaging with Fura-2-AM

For Ca^{2+} imaging, as described previously [65], Jurkat T cells were loaded with 1 µM Fura-2-AM in RPMI 1640 with 10% FCS at room temperature for 25 min. Then cells were washed with centrifugation, resuspended in 1 mM Ca^{2+} Ringer's solution, and seeded on poly(acrylamide) (PAAm) hydrogel substrate if not otherwise mentioned. Afterwards, Ca^{2+} imaging is acquired immediately. Fluorescence was emitted by 340 nm or 380 nm and infrared images were taken every 5 sec for 25 min at room temperature. The captured images were analyzed by T.I.L.L. Vision software. The traces were analyzed with the software Igor Pro6. For the experiment with BTP-2, all solutions contain 10 µM BTP-2 or the vehicle. The response time is defined as the time period between cell docking on the substrate and Ca^{2+} influx. The cells showing elevated Ca^{2+} levels ($[Ca^{2+}]_{int}$ exceeding the threshold Ratio 340/380=0.3) were defined as responsive cells. Time 0 of T cell activation is defined as the time point immediately before the $[Ca^{2+}]$int exceeds the threshold (Ratio 340/380=0.3). The peak was defined as the maximum value of ratio 340nm/380nm within the first 60 sec after the T cell activation. The plateau levels the average of 340nm/380nm ratios from the last 30 sec.

Conjugation of T cells with target cells

Target cells (NALM-6 or Raji cells) were pulsed with staphylococcal enterotoxin A (SEA, 0.1 µg/ml) and SEB (0.1 µg/ml) at 37°C for 40 min. For conjugation, Jurkat T cells and pulsed target cells were mixed and settled on the fibronectin (0.1 mg/ml)-coated coverslip at 37°C for 15 min. To reduce the stiffness of target cells, following SEA/SEB pulsing, NALM-6 cells were loaded with EGTA-AM (500 µM) at 37°C for 30 min and then washed twice to remove unloaded EGTA-AM.

Preparation and biofunctionalization of substrates

For Ca^{2+} imaging, poly (acrylamide-co-acrylic acid) (PAAm-co-AA) hydrogels with stiffness levels of 2, 12, and 50 kPa were prepared and functionalized following a previously described protocol [41]. Briefly, a mixture of AAm monomer and bis-AAm crosslinker was prepared with varying ratios, while maintaining a constant ratio of AA. Hydrogel discs were formed between two glass coverslips. The PAAm-co-AA hydrogels were firstly functionalized with biotin-PEG8-NH2 through an EDC/NHS activation step as follows. The PAAm-co-AA film was covered with 100 µL EDC/NHS solution (39 mg/12 mg in 0.1 M, pH 4.5 MES buffer) for 15 min, washed thoroughly with PBS and then directly incubated with 100 µL of biotin-PEG8-NH2 (1 mg/mL) solution in a petri dish for 2 hr at RT. The functionalized hydrogels underwent a triple wash with PBS and were stored in PBS at 4°C until use. Subsequently, the hydrogels of varying stiffness were incubated with streptavidin solution (100 µL, 100 µg/mL) for 1 –1.5 h (2 kPa) or 2.5 –3 h (12 and 50 kPa). These hydrogels were then subjected to overnight incubation with biotinylated anti-CD3 antibody (100 µg/mL, 30 µL) or IgG isotype (100 µg/mL, 30 µL) at 4°C.

For immunostaining and live-cell imaging, CytoSoft® Imaging 96-Well plates with stiffness of 2, 16 and 64 kPa from Advanced BioMatrix were used if not otherwise mentioned. Plates were coated with biotinylated anti-CD3 antibody (30 µg/mL, 50 µL/well) in PBS at 4°C for overnight. Afterwards, the antibody solution was removed and washed with PBS 3 times. For examining coating efficiency, Alexa Fluor® 488-conjugated anti-CD3 antibody (30 µg/mL, 50 µL/well) were used to coating the wells. The antibody density on the substrate was assessed the fluorescence intensity of Alexa Fluor® 488 with CellDiscover7 (20× objective, NA:0.7).

R*NA-seq data collection*

The sequencing data of human primary $CD4^+$ T cells [66] were obtained from the GSE217904 dataset available in the Gene Expression Omnibus. The GSE217904 dataset comprises 43 samples of primary human $CD4^+$ T-cells isolated from peripheral blood of either healthy individuals or patients with asthma [66]. For our analysis, we specifically selected gene expression profiles from all 10 samples of healthy donors. The original sequencing data of Jurkat T-cells [67] were collected from E-MTAB-7721 dataset at the European Nucleotide Archive. The data were then processed with Geneious Prime (2024.0). The levels of mRNA are shown as TPM (Transcripts Per Million).

Fluorescence-based Ca^{2+} imaging with Fluo-4-AM and MTOC translocation

Jurkat T cells were loaded with 1 µM Fluo-4-AM and SPY650-tubulin (1:2000) in RPMI 1640 with 10% FCS at 37°C, 5% CO_2 in a humidified incubator for 25 min. 1 µM GsMTx-4 or the vehicle is present in all solutions. After staining, cells were washed with centrifugation. Cells were mixed with 1 mM Ca^{2+} Ringer's solution and plated into biotin anti-human CD3 Antibody coated CytoSoft® Imaging 96-Well Plate. Afterwards, images were acquired with a Zeiss Cell Observer HS system with a 20× alpha objective and an AxioCam MRm Rev. 3. During the experiment, the fluorescence of Fluo-4 was emitted by 470 nm and acquired with a 38HE filter set. The fluorescence of tubulin was emitted by 625 nm and acquired with a Cy5 (F36-523) filter set with 1 µm z-step size. The images were acquired every 9 sec at room temperature. The fluorescence of Fluo-4 was quantified with Imaris. The position of MTOC was defined with TrackMate of Fiji Plugins.

Epifluorescence deconvolution microscopy and immunofluorescence

For substrates, T cells were settled on antibody-coated substrates at 37°C for the indicated periods of time. For conjugation, T cells were settled with SEA/SEB-pulsed target cells (NALM-6 cells or Raji cells) on fibronectin (0.1 mg/ml)-coated coverslips at 37°C for 15 min. Cells were then fixed with 4% paraformaldehyde and permeabilized with 0.3% Triton-100 except for γ-tubulin antibody (permeabilized with methanol/acetone solution at -20°C for 20 min. After immune staining, the fixed samples were measured with a Zeiss Cell Observer HS system containing GFP (38HE; Zeiss), ET-Texas Red (Chroma Technology), DAPI HE (Zeiss), Texas Red HE (Zeiss), and Cy 5 HE (Zeiss) filter sets. The samples on PAAm hydrogel were measured with alpha Plan-Apochromat 63x/1.40 Oil DIC M27. The samples on the coverslip were measured with alpha Plan-Apochromat 63x/1.40

Oil DIC M27. The samples in CytoSoft® Imaging 96-Well Plates were measured with Fluar 40x/1.30 Oil M27. The acquired images were preceded for deconvolution with the Huygens Essential program by using a theoretical point spread function.

Immunostaining and flow cytometry

Samples were fixed with 4% paraformaldehyde (PFA) and then washed twice with PBS/0.5% BSA. Cells were permeabilized and blocked with 0.3% Triton-100 in PBS containing 5% FCS and 0.5% BSA for 30 min at room temperature. And then cells were stained with the indicated primary antibody for 1 hr at room temperature followed by staining of Alexa Fluor™ 647 labeled secondary antibody. Flow cytometry data were acquired using a FACSVerse™ flow cytometer (BD Biosciences) and were analyzed with FlowJo v10 (FLOWJO, LLC).

Real-time deformability cytometry (RT-DC)

To assess the stiffness of NALM-6 cells RT-DC (Zellmechanik Dresden) was used [40]. NALM-6 cells were either treated with DMSO or EGTA-AM for 30 min after which they were resuspended in 100 µl of Cell Carrier B solution (phosphate-buffered saline with the addition of long-chain methylcellulose polymers of 0.6 w/v%). A microfluidic PDMS chip with a 300 µm long central constriction of 30 µm×30 µm cross-section was assembled on the stage of an inverted microscope (Zeiss). The cell suspension was loaded on the chip using a syringe pump. The cells flowing through the microfluidic channel deform due to the shear stresses and pressure gradient caused by the flow profile [40]. Each event is imaged live using a CMOS camera and analyzed in real-time. Events were acquired at a flowrate of 0.12 µl/s. The mechanical properties of the cells were analyzed using ShapeOut 2 (Zellmechanik Dresden) which employs linear mixed models to calculate statistical significances.

Statistical Analysis

Data are presented as mean. GraphPad Prism 6 Software (San Diego, CA, USA) was used for statistical analysis. If the number of data points is smaller than 8, the differences between 2 columns were analyzed by the Student's t-test. Otherwise, the data were first examined for Gaussian distribution. If the dataset fits Gaussian distribution, the differences between 2 columns were analyzed with the Student's t-test, otherwise with the Mann-Whitney test. the differences between 3 columns were analyzed by the One-way ANOVA or nonparametric test. If datasets fit Gaussian distribution, the differences between 3 columns were analyzed with a one-way ANOVA with Tukey's multiple comparisons, otherwise the differences between 3 columns were analyzed with the Krushal-Wallis test with Dunn's multiple comparisons. The RT-DC data were analyzed with linear mixed-effect models.

Ethical Considerations

Research carried out for this study with healthy donor material (leukocyte reduction system chambers from human blood donors) is authorized by the local ethic committee [declaration from 16.4.2015 (84/15; Prof. Dr. Rettig-Stürmer)].

Acknowledgments

We thank Prof. Hermann Eichler (Institute of Clinical Hemostaseology and Transfusion Medicine) for blood samples; Carmen Hässig, Cora Hoxha, Gertrud Schäfer, Sandra Janku, and Kathleen Seelert for excellent technical help; Britta Abt and Jennifer Kasper for helping in hydrogels; Adolfo Cavalié for providing NALM-6 cells; Dalia Alansary for Ca^{2+} imaging; Galia Montalvo and Franziska Lautenschläger for their kind assistance in RT-DC; Hong Zhang for helping in immunostaining. This project was funded by the Deutsche Forschungsgemeinschaft, SFB 1027 (Projects A2 (BQ), A11 (MH), and B6 (AdC) and "Large Equipment Grants" (GZ: INST 256/419-1 FUGG for the lightsheet

microscope, GZ: INST 256/423-1 FUGG for the flow cytometer, GZ: INST 256/429-1 FUGB for ImageXpress, and GZ: INST 256/555-1 FUGG for the Celldiscoverer 7), Miniproposal of SFB 1027 (to R.Z.).

References

1. Guck, J. *et al.* Optical deformability as an inherent cell marker for testing malignant transformation and metastatic competence. *Biophys J* **88**, 3689-3698 (2005).

2. Xu, W. *et al.* Cell stiffness is a biomarker of the metastatic potential of ovarian cancer cells. *PLoS One* **7**, e46609 (2012).

3. Hayashi, K. & Iwata, M. Stiffness of cancer cells measured with an AFM indentation method. *J Mech Behav Biomed Mater* **49**, 105-111 (2015).

4. Fuhs, T. *et al.* Rigid tumours contain soft cancer cells. *Nat Phys* **18** (2022).

5. Lv, J. *et al.* Cell softness regulates tumorigenicity and stemness of cancer cells. *EMBO J* **40**, e106123 (2021).

6. Rianna, C., Radmacher, M. & Kumar, S. Direct evidence that tumor cells soften when navigating confined spaces. *Molecular Biology of the Cell* **31**, 1726-1734 (2020).

7. Stinchcombe, J.C. & Griffiths, G.M. Secretory mechanisms in cell-mediated cytotoxicity. *Annu Rev Cell Dev Biol* **23**, 495-517 (2007).

8. Dustin, M.L. & Long, E.O. Cytotoxic immunological synapses. *Immunol Rev* **235**, 24-34 (2010).

9. Stinchcombe, J.C., Majorovits, E., Bossi, G., Fuller, S. & Griffiths, G.M. Centrosome polarization delivers secretory granules to the immunological synapse. *Nature* **443**, 462-465 (2006).

10. Yi, J. *et al.* Centrosome repositioning in T cells is biphasic and driven by microtubule end-on capture-shrinkage. *J Cell Biol* **202**, 779-792 (2013).

11. Ritter, A.T. *et al.* Actin depletion initiates events leading to granule secretion at the immunological synapse. *Immunity* **42**, 864-876 (2015).

12. Radoja, S. *et al.* CD8(+) tumor-infiltrating T cells are deficient in perforin-mediated cytolytic activity due to defective microtubule-organizing center mobilization and lytic granule exocytosis. *J Immunol* **167**, 5042-5051 (2001).

13. Quann, E.J., Merino, E., Furuta, T. & Huse, M. Localized diacylglycerol drives the polarization of the microtubule-organizing center in T cells. *Nat Immunol* **10**, 627-635 (2009).

14. Martin-Cofreces, N.B. *et al.* MTOC translocation modulates IS formation and controls sustained T cell signaling. *J Cell Biol* **182**, 951-962 (2008).

521 15. Hogan, P.G. Calcium-NFAT transcriptional signalling in T cell activation and T cell
522 exhaustion. *Cell Calcium* **63**, 66-69 (2017).

523 16. Macian, F. NFAT proteins: key regulators of T-cell development and function. *Nat Rev*
524 *Immunol* **5**, 472-484 (2005).

525 17. Martinez, G.J. *et al.* The transcription factor NFAT promotes exhaustion of activated
526 CD8(+) T cells. *Immunity* **42**, 265-278 (2015).

527 18. Hogan, P.G., Chen, L., Nardone, J. & Rao, A. Transcriptional regulation by calcium,
528 calcineurin, and NFAT. *Genes Dev* **17**, 2205-2232 (2003).

529 19. Rao, A. Signaling to gene expression: calcium, calcineurin and NFAT. *Nat Immunol* **10**, 3-
530 5 (2009).

531 20. Timmerman, L.A., Clipstone, N.A., Ho, S.N., Northrop, J.P. & Crabtree, G.R. Rapid
532 shuttling of NF-AT in discrimination of Ca2+ signals and immunosuppression. *Nature*
533 **383**, 837-840 (1996).

534 21. Feske, S., Draeger, R., Peter, H.H., Eichmann, K. & Rao, A. The duration of nuclear
535 residence of NFAT determines the pattern of cytokine expression in human SCID T cells.
536 *J Immunol* **165**, 297-305 (2000).

537 22. Feske, S., Giltnane, J., Dolmetsch, R., Staudt, L.M. & Rao, A. Gene regulation mediated
538 by calcium signals in T lymphocytes. *Nat Immunol* **2**, 316-324 (2001).

539 23. Kupfer, A., Dennert, G. & Singer, S.J. The reorientation of the Golgi apparatus and the
540 microtubule-organizing center in the cytotoxic effector cell is a prerequisite in the lysis
541 of bound target cells. *J Mol Cell Immunol* **2**, 37-49 (1985).

542 24. Ostergaard, H. & Clark, W.R. The role of Ca2+ in activation of mature cytotoxic T
543 lymphocytes for lysis. *J Immunol* **139**, 3573-3579 (1987).

544 25. Vaeth, M., Kahlfuss, S. & Feske, S. CRAC Channels and Calcium Signaling in T Cell-
545 Mediated Immunity. *Trends Immunol* **41**, 878-901 (2020).

546 26. Cahalan, M.D. & Chandy, K.G. The functional network of ion channels in T lymphocytes.
547 *Immunol Rev* **231**, 59-87 (2009).

548 27. Shaw, P.J., Qu, B., Hoth, M. & Feske, S. Molecular regulation of CRAC channels and their
549 role in lymphocyte function. *Cell Mol Life Sci* **70**, 2637-2656 (2013).

550 28. Parekh, A.B. & Putney, J.W., Jr. Store-operated calcium channels. *Physiol Rev* **85**, 757-
551 810 (2005).

552 29. Hogan, P.G., Lewis, R.S. & Rao, A. Molecular basis of calcium signaling in lymphocytes:
553 STIM and ORAI. *Annu Rev Immunol* **28**, 491-533 (2010).

554 30. McCarl, C.A. *et al.* ORAI1 deficiency and lack of store-operated Ca2+ entry cause
555 immunodeficiency, myopathy, and ectodermal dysplasia. *J Allergy Clin Immunol* **124**,
556 1311-1318 e1317 (2009).

557 31. Feske, S., Picard, C. & Fischer, A. Immunodeficiency due to mutations in ORAI1 and
558 STIM1. *Clin Immunol* **135**, 169-182 (2010).

559 32. Shaw, P.J. & Feske, S. Regulation of lymphocyte function by ORAI and STIM proteins in
560 infection and autoimmunity. *J Physiol* **590**, 4157-4167 (2012).

561 33. Ridone, P., Vassalli, M. & Martinac, B. Piezo1 mechanosensitive channels: what are they
562 and why are they important. *Biophys Rev* **11**, 795-805 (2019).

563 34. Coste, B. *et al.* Piezo1 and Piezo2 are essential components of distinct mechanically
564 activated cation channels. *Science* **330**, 55-60 (2010).

565 35. Liu, C.S.C. *et al.* Cutting Edge: Piezo1 Mechanosensors Optimize Human T Cell Activation.
566 *J Immunol* **200**, 1255-1260 (2018).

567 36. Jairaman, A. *et al.* Piezo1 channels restrain regulatory T cells but are dispensable for
568 effector CD4(+) T cell responses. *Sci Adv* **7** (2021).

569 37. Liu, C.S.C. *et al.* Piezo1 mechanosensing regulates integrin-dependent chemotactic
570 migration in human T cells. *bioRxiv* (2022).

571 38. Hope, J.M. *et al.* Fluid shear stress enhances T cell activation through Piezo1. *BMC Biol*
572 **20**, 61 (2022).

573 39. Du, H. *et al.* Tuning immunity through tissue mechanotransduction. *Nat Rev Immunol*
574 **23**, 174-188 (2023).

575 40. Otto, O. *et al.* Real-time deformability cytometry: on-the-fly cell mechanical
576 phenotyping. *Nat Methods* **12**, 199-202, 194 p following 202 (2015).

577 41. Zhang, J. *et al.* Micropatterned soft hydrogels to study the interplay of receptors and
578 forces in T cell activation. *Acta Biomater* **119**, 234-246 (2021).

579 42. Quintana, A. *et al.* Calcium microdomains at the immunological synapse: how ORAI
580 channels, mitochondria and calcium pumps generate local calcium signals for efficient T-
581 cell activation. *EMBO J* **30**, 3895-3912 (2011).

582 43. Kar, P. *et al.* Dynamic assembly of a membrane signaling complex enables selective
583 activation of NFAT by Orai1. *Curr Biol* **24**, 1361-1368 (2014).

584 44. Yoast, R.E. *et al.* The native ORAI channel trio underlies the diversity of Ca(2+) signaling
585 events. *Nat Commun* **11**, 2444 (2020).

586 45. Zitt, C. *et al.* Potent inhibition of Ca2+ release-activated Ca2+ channels and T-
587 lymphocyte activation by the pyrazole derivative BTP2. *J Biol Chem* **279**, 12427-12437
588 (2004).

589 46. Ishikawa, J. *et al.* A pyrazole derivative, YM-58483, potently inhibits store-operated
590 sustained Ca2+ influx and IL-2 production in T lymphocytes. *J Immunol* **170**, 4441-4449
591 (2003).

592 47. Yoo, S., Mittelstein, D.R., Hurt, R.C., Lacroix, J. & Shapiro, M.G. Focused ultrasound
593 excites cortical neurons via mechanosensitive calcium accumulation and ion channel
594 amplification. *Nat Commun* **13**, 493 (2022).

595 48. Zheng, Y. *et al.* Optoregulated force application to cellular receptors using molecular
596 motors. *Nat Commun* **12**, 3580 (2021).

597 49. Kim, S.T. *et al.* The alphabeta T cell receptor is an anisotropic mechanosensor. *J Biol*
598 *Chem* **284**, 31028-31037 (2009).

599 50. Liu, B., Kolawole, E.M. & Evavold, B.D. Mechanobiology of T Cell Activation: To Catch a
600 Bond. *Annu Rev Cell Dev Biol* **37**, 65-87 (2021).

601 51. Jenkins, M.R. & Griffiths, G.M. The synapse and cytolytic machinery of cytotoxic T cells.
602 *Curr Opin Immunol* **22**, 308-313 (2010).

603 52. Huse, M. Microtubule-organizing center polarity and the immunological synapse:
604 protein kinase C and beyond. *Front Immunol* **3**, 235 (2012).

605 53. Combs, J. *et al.* Recruitment of dynein to the Jurkat immunological synapse. *Proc Natl*
606 *Acad Sci U S A* **103**, 14883-14888 (2006).

607 54. Hartzell, C.A., Jankowska, K.I., Burkhardt, J.K. & Lewis, R.S. Calcium influx through CRAC
608 channels controls actin organization and dynamics at the immune synapse. *Elife* **5**
609 (2016).

610 55. Waldman, A.D., Fritz, J.M. & Lenardo, M.J. A guide to cancer immunotherapy: from T cell
611 basic science to clinical practice. *Nature Reviews Immunology* **20**, 651-668 (2020).

612 56. Wherry, E.J. & Kurachi, M. Molecular and cellular insights into T cell exhaustion. *Nat Rev*
613 *Immunol* **15**, 486-499 (2015).

614 57. Malko, P., Jia, X., Wood, I. & Jiang, L.H. Piezo1 channel-mediated Ca(2+) signaling
615 inhibits lipopolysaccharide-induced activation of the NF-kappaB inflammatory signaling
616 pathway and generation of TNF-alpha and IL-6 in microglial cells. *Glia* **71**, 848-865
617 (2023).

618 58. Zhang, X. *et al.* Piezo1-mediated mechanosensation in bone marrow macrophages
619 promotes vascular niche regeneration after irradiation injury. *Theranostics* **12**, 1621-
620 1638 (2022).

621 59. Zhou, T. *et al.* Piezo1/2 mediate mechanotransduction essential for bone formation
622 through concerted activation of NFAT-YAP1-ss-catenin. *Elife* **9** (2020).

623 60. Caulier, A. *et al.* PIEZO1 activation delays erythroid differentiation of normal and
624 hereditary xerocytosis-derived human progenitor cells. *Haematologica* **105**, 610-622
625 (2020).

626 61. Li, R. *et al.* Identification of Piezo1 as a potential target for therapy of colon cancer stem-
627 like cells. *Discov Oncol* **14**, 95 (2023).

628 62. Yu, Z. *et al.* Piezo1 is the cardiac mechanosensor that initiates the cardiomyocyte
629 hypertrophic response to pressure overload in adult mice. *Nat Cardiovasc Res* **1**, 577–
630 591 (2022).

631 63. Li, R., Ma, C., Cai, H. & Chen, W. The CAR T-Cell Mechanoimmunology at a Glance. *Adv*
632 *Sci (Weinh)* **7**, 2002628 (2020).

633 64. Wang, J.H. T cell receptors, mechanosensors, catch bonds and immunotherapy. *Prog*
634 *Biophys Mol Biol* **153**, 23-27 (2020).

635 65. Alansary, D., Bogeski, I. & Niemeyer, B.A. Facilitation of Orai3 targeting and store-
636 operated function by Orai1. *Biochim Biophys Acta* **1853**, 1541-1550 (2015).

637 66. Tutino, M. *et al.* Identification of differences in CD4(+) T-cell gene expression between
638 people with asthma and healthy controls. *Sci Rep* **13**, 22796 (2023).

639 67. Quentmeier, H. *et al.* The LL-100 panel: 100 cell lines for blood cancer studies. *Sci Rep* **9**,
640 8218 (2019).

641

642

643

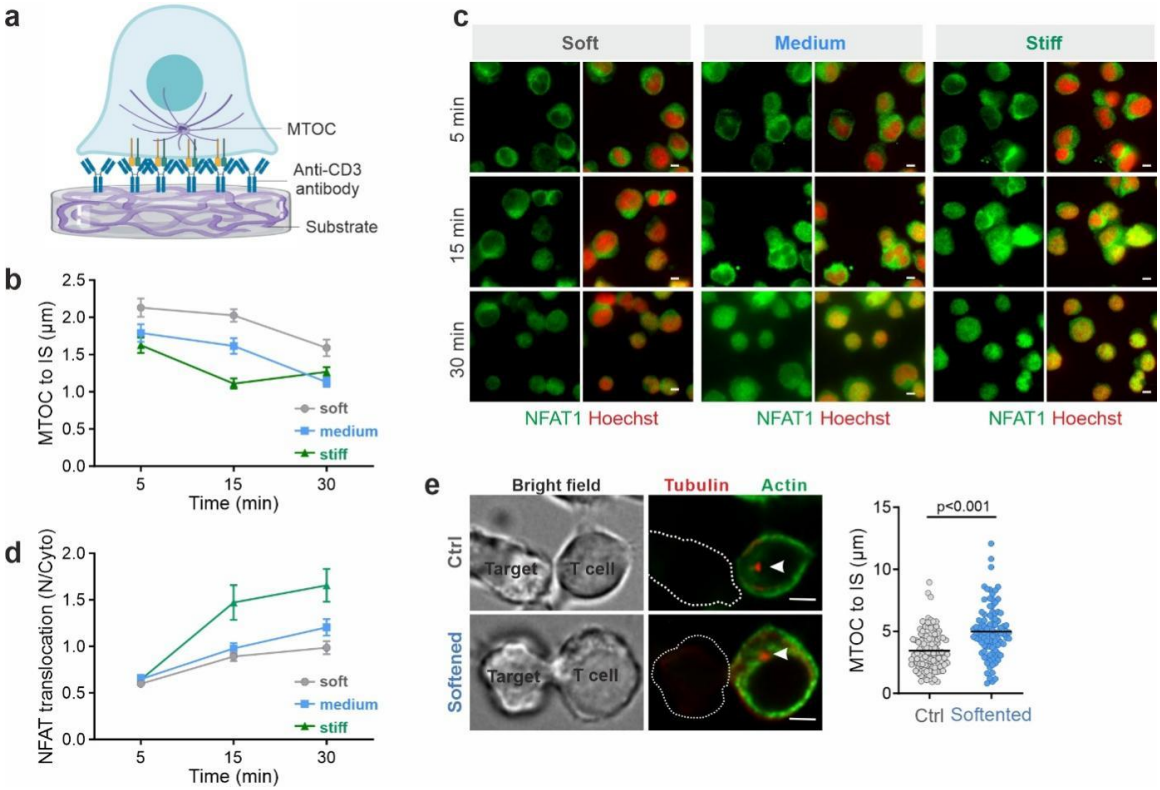

Figure 1. The impact of target cell stiffness on MTOC reorientation and NFAT nuclear translocation. (**a**) Schematic of anti-CD3 antibody-coated hydrogel with T cell contact. (**b-d**) Stiffness influences MTOC reorientation and NFAT translocation in Jurkat T cells on substrates. Jurkat T cells were settled on functionalized substrates for varying time periods at 37°C before fixation. (**b**) MTOC was stained with the anti-tubulin antibody and the position of the IS was identified with Phalloidin-labeled actin. (**c, d**) NFAT and the nucleus were labelled with anti-NFAT antibody and Hoechst 33342, respectively. (**e**) Softening of cancer cells hinders MTOC translocation. NALM-6 cells were pre-treated with 500 µM EGTA-AM for 30 min at 37°C. Jurkat T cells were conjugated with target cells at 37°C for 15 min before fixation. The MTOC was stained with anti-tubulin antibody and indicated with white arrowheads. 96-well CytoSoft plates were used for soft (2 kPa), medium (16 kPa), and stiff (64 kPa) substrates. Student's t-test was conducted for **e**. The data are shown as mean±SEM in **b** and **d**. Scale bars are 5 µm. All the results are from at least three independent experiments.

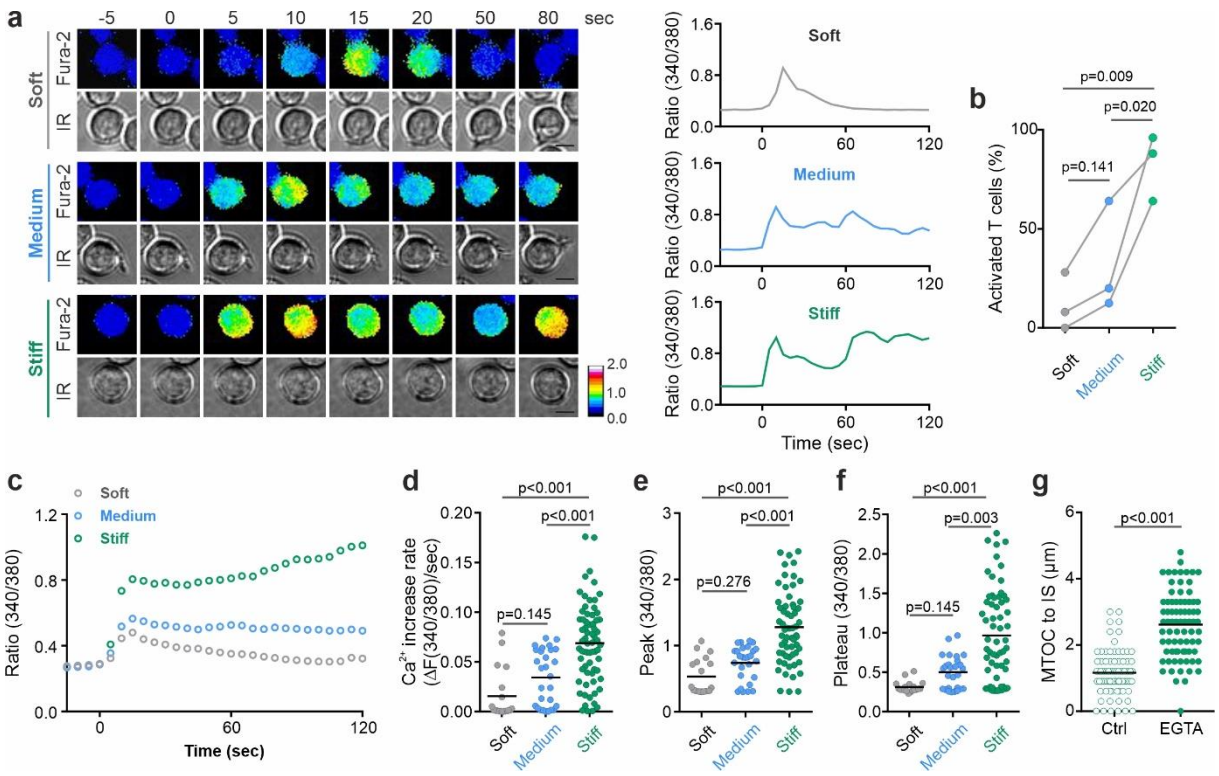

Figure 2. TCR activation triggered Ca^{2+} rise is modulated by substrate stiffness and is required for MTOC reorientation. (**a-f**) Jurkat T cells were loaded with Fura-2 and settled on anti-CD3 antibody functionalized hydrogels. Live-cell imaging with 340 nm, 380 nm, and infrared (IR) was acquired every 5 sec at RT. Exemplary cells and the corresponding Ca^{2+} signals are presented in **a**; IR: Infrared. The fractions of responsive T cells showing elevated $[Ca^{2+}]_{int}$ after gel contact are shown in **b**, with each dot representing one experiment. Scale bars are 5 µm. Mean values of all responsive cells are shown in **c**, in which time 0 is defined as the time point immediately before the $[Ca^{2+}]_{int}$ exceeds the threshold (Ratio 340/380=0.3). Ca^{2+} increase rates (**d**), peak (**e**), and plateau (**f**) were quantified for responsive cells. (**g**) Extracellular Ca^{2+} depletion hinders MTOC reorientation. Jurkat T cells were settled on anti-CD3 antibody functionalized stiff substrates (64 kPa) in the presence or absence of EGTA (0.5 mM) for 15 min before fixation. MTOC was stained with the anti-tubulin antibody and the position of the IS was identified with phalloidin-labeled actin. Results are from three independent experiments. A one-way ANOVA test with Holm-Sidak's multiple comparisons was conducted for **a**. A Krushal-Wallis test with Dunn's multiple comparisons was conducted for **d, f**. A one-way ANOVA test with Tukey's multiple comparisons and the Mann-Whitney test was conducted for **e** and **g**, respectively. Functionalized hydrogels with stiffness levels of 2 kPa (soft), 12 kPa (medium), and 50 kPa (stiff) were used in a-f. 96-well CytoSoft plates with a stiffness level of 64 kPa (stiff) were used in g. All the results are from at least three independent experiments.

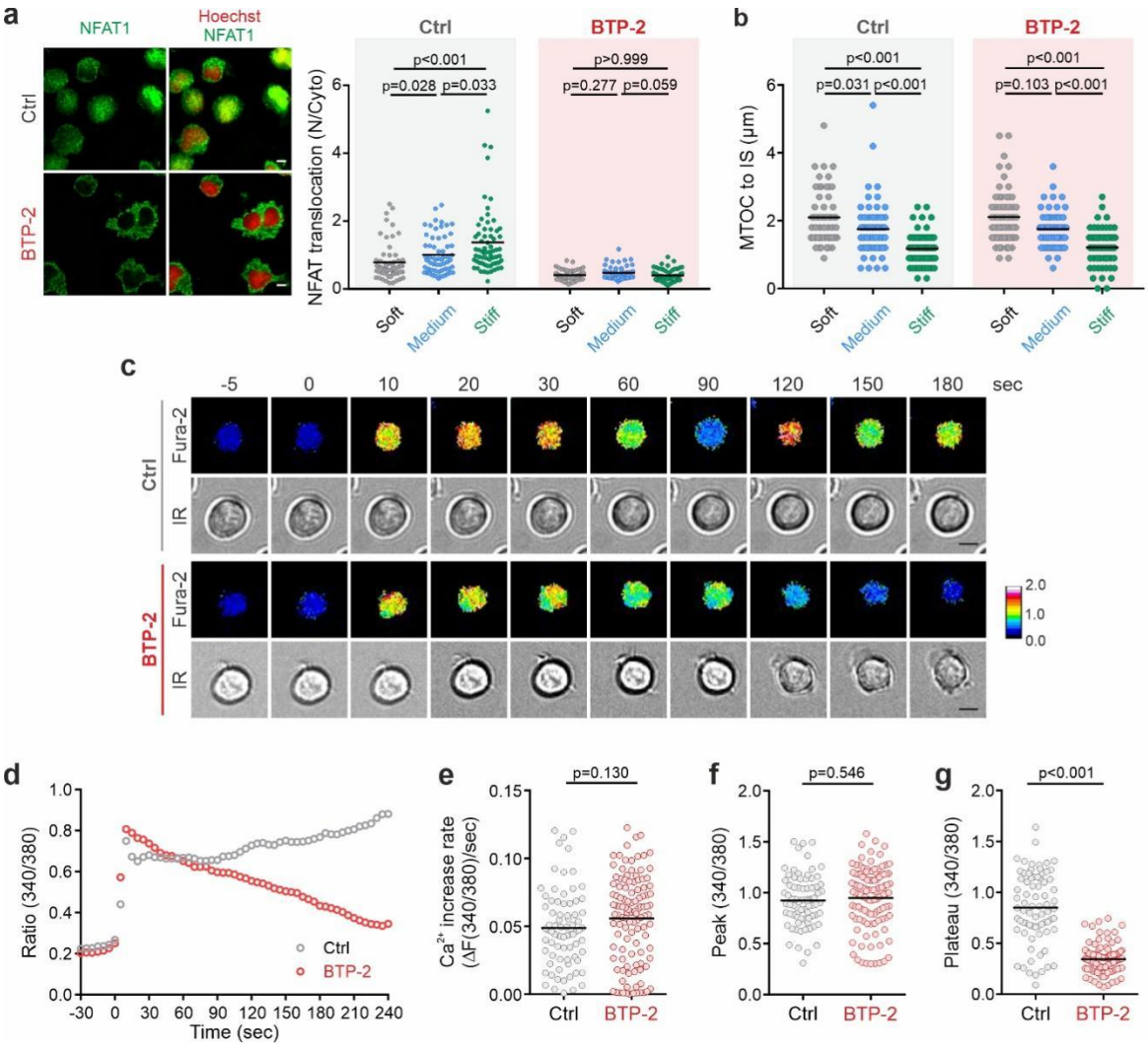

Figure 3. CRAC channels are crucial for stiffness-dependent NFAT nuclear translocation and the maintenance of elevated $[Ca^{2+}]_{int}$. Jurkat T cells were pre-treated with BTP-2 (10 µM) at 37°C for 30 min. Subsequently, T cells were loaded with Fura-2-AM and settled on anti-CD3-antibody functionalized substrates in the presence with BTP-2 (10 µM) for Ca^{2+} imaging. (**a**) Orai1 governs stiffness dependent NFAT translocation. NFAT and the nucleus were stained with anti-NFAT antibody and Hoechst 33342, respectively. Exemplary cells on stiff substrates are shown. (**b**) Orai1 is not involved in MTOC reorientation. MTOC was stained with the anti-tubulin antibody and the position of the IS was identified with Phalloidin-labeled actin. (**c-g**) Impact of Orai1 channels on TCR activation-triggered Ca^{2+} rise. Jurkat T cells were settled on stiff substrates. Exemplary cells are shown in **c** (IR: infrared). The mean values of all responsive cells for each condition are shown in **d**, in which time 0 is defined as the time point immediately before the $[Ca^{2+}]_{int}$ exceeds the threshold (Ratio 340/380=0.3). Ca^{2+} increase rate (**e**), peak (**f**), and plateau (**g**) were quantified for individual cells. Scale bars are 5 µm. All results are from three independent experiments. A Krushal-Wallis test with Dunn's multiple comparisons test was conducted for **a, b**. A Mann-Whitney

test was conducted for **e-g**. 96-well CytoSoft plates were used for soft (2 kPa), medium (16 kPa), and stiff (64 kPa) substrates. All the results are from at least three independent experiments.

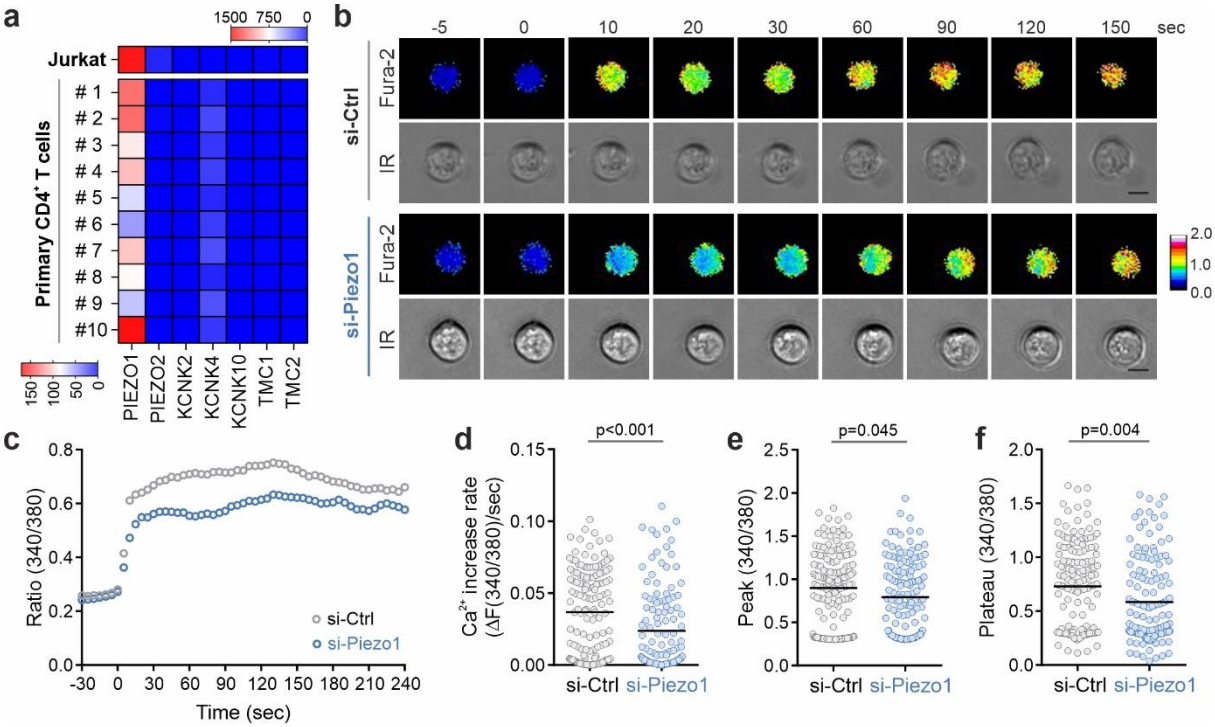

Figure 4. Piezo1 regulates Ca^{2+} increase rates. (**a**) Expression of mechano-sensitive ion channels in T cells. The levels of mRNA were identified with RNA-sequencing for Jurkat T-cells [67] and primary human $CD4^+$ T cells (from 10 healthy individuals) [66] and are shown as Transcripts Per Million. (**b-f**) Impact of Piezo1 on TCR activation-triggered Ca^{2+} rise. Jurkat T cells transfected with siRNA were loaded with Fura-2-AM and then settled on anti-CD3 antibody functionalized stiff hydrogels (50 kPa). Exemplary cells are shown in **b** (IR: infrared). Scale bars are 5 µm. Averaged curves of all responsive cells for each condition are shown in **c**, in which time 0 is defined as the time point immediately before the $[Ca^{2+}]_{int}$ exceeds the threshold (ratio 340/380=0.3). Ca^{2+} increase rate (**d**), peak (**e**), and plateau (**f**) were quantified for individual cells. A Mann-Whitney test was conducted for **d-f**. All results are from three independent experiments.

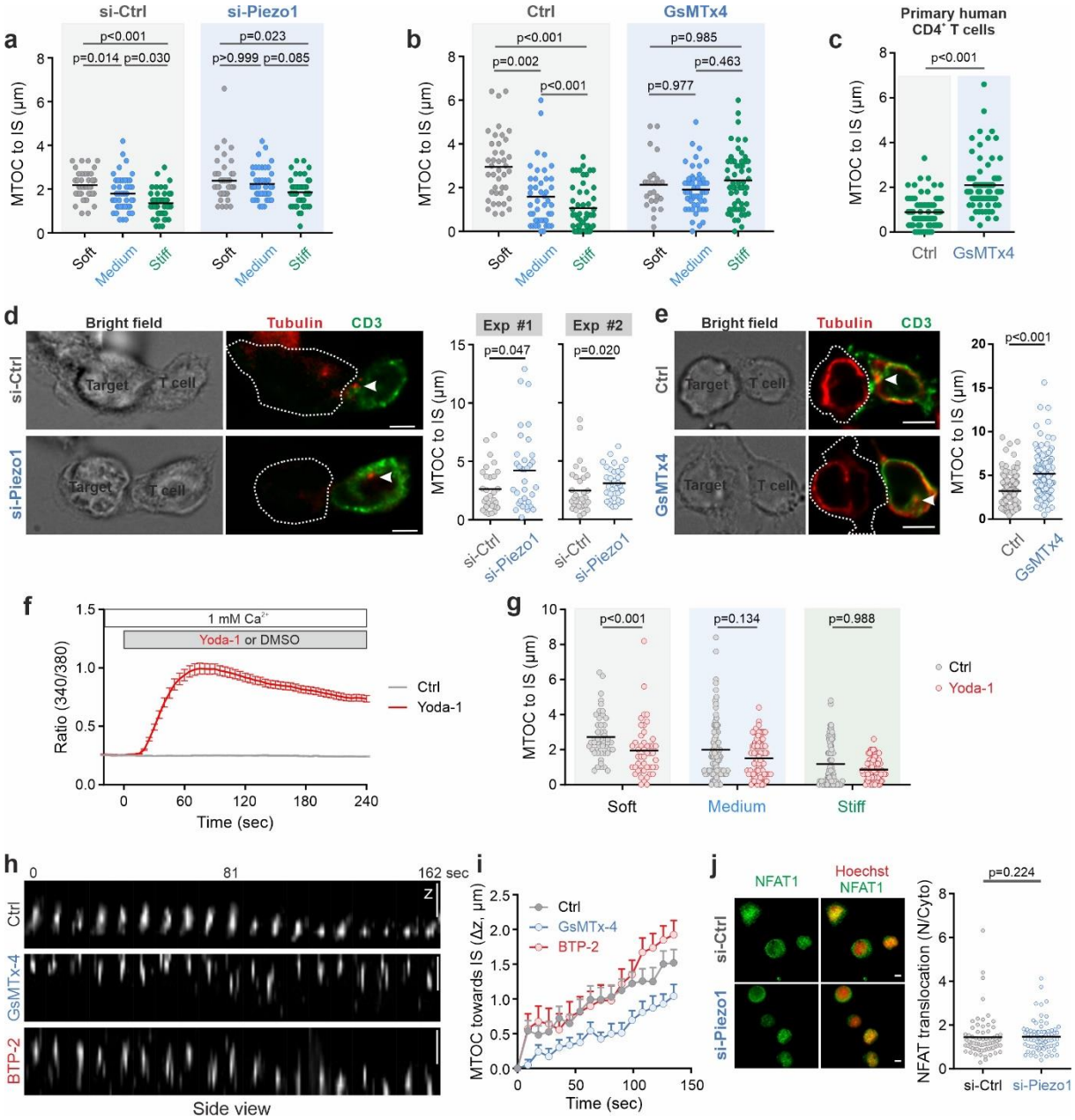

Figure 5. Piezo1 plays a pivotal role for MTOC reorientation but not for NFAT translocation. (**a-e**) Perturbation of Piezo1 hinders stiffness-dependent MTOC reorientation. Jurkat T cells (**a**, **b**, **d**, **e**) or primary human CD4$^+$ T cells (**c**) were used. T cells were either transfected with siRNA (**a**, **d**) or treated with GsMTx-4 (1 µM) (**b**, **c**, **e**). In **a-c**, T cells were settled on anti-CD3-antibody functionalized substrates. In **d**-**e**, T cells were conjugated with SEA/SEB pulsed target cells, either NALM-6 cells (**d**) or Raji cells (**e**), at 37°C for 15 min before fixation. MTOC was stained with the anti-tubulin antibody. The position of the IS was identified with phalloidin-labeled actin. White arrowheads in **d** and **e** highlight the position of MTOC (**f**) Yoda-1 treatment induces Ca^{2+} influx in T cells. Jurkat T cells loaded with Fura-2-AM were settled on poly-L-ornithine-coated coverslips in 1 mM Ca^{2+} ringer solution. Yoda-1 (15 µM) was perfused at the time 0. (**g**) Activation of Piezo1 sensitizes MTOC reorientation on soft substrates. Jurkat T cells were settled on anti-CD3-antibody functionalized substrates in the presence of Yoda-1 (15 µM) at 37°C for 15 min before fixation.

MTOC was stained with anti-γ-tubulin antibodies, and T cell contour was indicated with Phalloidin-labeled actin. (**h-i**) Piezo1 but not CRAC/Orai1 governs MTOC reorientation. Jurkat T cells were pre-treated with GsMTx-4 (1 µM), BTP-2 (10 µM) or vehicle control (Ctrl) at 37°C for 30 min. MTOC was stained by SPY650-tublin and visualized every 9 sec for 30 min at RT on anti-CD3-antibody-functionalized stiff substrates (64 kPa). (**j**) Piezo1 has no impact on NFAT nuclear translocation. Jurkat T cells transfected with siRNA were settled on anti-CD3-antibody-functionalized stiff substrates (64 kPa) at 37°C for 15 min before fixation. NFAT1 was labeled using anti-NFAT1 antibodies, and the nucleus was labelled with Hoechst 33342. A Krushal-Wallis test with Dunn's multiple comparisons was conducted for **a**. A one-way ANOVA with Tukey's multiple comparisons was conducted for **b**. A Mann-Whitney test was conducted for **c**, **d, e,** and **j**. In **a**, 96-well CytoSoft plates with stiff levels of 2 kPa (soft), 16 kPa (medium), and 64 kPa (stiff) were used. In **b** and **g**, functionalized hydrogels with stiffness levels of 2 kPa (soft), 12 kPa (medium), and 50 kPa (stiff) were used. In **c** and **h-j**, 96-well CytoSoft plates with 64 kPa (stiff) were used. Scale bars are 5 µm. In all scatter dot plots, one dot indicates one cell. In **i**, the data are shown as mean±SEM (Ctrl: 45 cells, GsMTx-4: 45 cells, BTP-2: 39 cells). Results in (**d**, **f, g**) were from two independent experiments. All other results were from three independent experiments or three donors.